Hot-Electron Conduction in the Lead Chalcogenides†

Hugues St-Onge* and J. N. Walpole‡
Department of Electrical Engineering and Center for Materials Science and Engineering, Massachusetts Institute of Technology, Cambridge, Massachusetts 02139
(Received 20 March 1972)

An experimental and theoretical investigation of hot-electron conduction in the lead chalcogenides is presented. Measurements of velocity-field characteristics have been performed on bulk samples of n-type PbSe, PbTe, and $Pb_{9.83}Sn_{0.17}Te$ at 77 and 4.2 °K for carrier concentrations ranging from 1×10^{17} to 5×10^{17} cm^{-3}. The results indicate that the dominant scattering mechanism at high electric fields is via polar-optical-phonon emission. The theory of Dumke for impact ionization which assumes a highly streamed distribution function is modified to take into account the ellipsoidal constant-energy surfaces of the lead chalcogenides. Generation rates are calculated for the three materials studied. At 77 °K the threshold electric fields for experimentally observable impact ionization are found to be 2500, 1050, and 550 V/cm for PbSe, PbTe, and $Pb_{0.83}Sn_{0.17}Te$, respectively. These results agree well with the theory even though the distribution function is not purely one dimensional.

I. INTRODUCTION

In recent years the study of high-electric-field transport in elemental semiconductors and in the III-V and II-VI compounds has been given considerable attention due to the availability of relatively pure material. Hot-electron conduction has been investigated in covalent semiconductors such as Ge[1] and Si[2] and in a variety of predominantly polar semiconductors including InSb,[3] InAs,[4] GaAs,[5] InP,[4] and CdTe.[4] Preliminary work on PbSe and PbTe was reported elsewhere by the authors.[6] Because of the difficulty of obtaining low carrier concentrations in the lead salts special experimental techniques have been used and are reviewed here in greater detail. The object of this paper is to present an experimental observation and theoretical interpretation of hot-electron conduction in PbSe, PbTe, and $Pb_{1-x}Sn_xTe$. For the first time[7] the process of impact ionization in bulk lead chalcogenides is investigated. The influence of the band gap reduction occurring in $Pb_{1-x}Sn_xTe$ alloys on the threshold for impact ionziation is also discussed.

When a polar semiconductor at low temperatures is subjected to a high electric field, the mobility first decreases because of the effectiveness of polar-optical-phonon emission as an energy-loss mechanism.[8] At higher fields depending on the size of the energy gap relative to the separation between the conduction band and subsidiary minima, impact ionization or the Gunn effect or both can occur. The two phenomena have been observed in InSb,[9] for example. The experimental and theoretical evidence presented here essentially demonstrates the occurrence of impact ionization in n-type lead chalcogenides. Speculations about a second valence band in PbTe have suggested the possibility of a Gunn effect in p-type PbTe. Because of the experimental difficulty of making Ohmic contacts to p-type material, this paper deals only with n-type materials.

The theoretical analysis of high-electric-field transport in semiconductors is in general a very difficult problem and only recently with the advent of simulation techniques such as the Monte Carlo[10] method or special iteration techniques[11] have satisfactory calculations been performed for materials such as GaAs,[12] InSb,[13] and Ge.[14] These numerical methods circumvent the problem of analytically solving the Boltzmann equation and have the advantage of always approaching the exact solution to the transport equation. Less exact but more readily usable methods are often useful in the interpretation of experimental data and make use of physical approximations to simplify the mathematical treatment. One such method using a Maxwellian distribution function displaced in momentum space was first applied to the case of polar semiconductors by Stratton.[15] It assumes that intercarrier collisions are sufficiently frequent to randomize both the energy and momentum distribution functions and is valid at electric fields below the impact-ionization regime. The theory of Stratton is reviewed here for the case of the lead salts, to establish the predominance of polar-optical-phonon scattering at high electric fields; its limitations are discussed in the light of the low-field scattering properties of the lead salts.

The problem of impact ionization was first treated for covalent semiconductors.[16–18] The theory of Baraff,[18] for example, has been used to calculate the ionization coefficient α in Ge and Si. Baraff's treatment and subsequently the theory of Keldysh[19] apply only to the case of isotropic scattering. In the Pb salts an electron loses energy

TABLE I. Low-field carrier concentration and Hall mobility at 77 °K of annealed semiconductors from which samples were fabricated.

Semiconductor	Concentration n_0 (cm^{-3})	Mobility (cm^2/V sec)
PbTe (*N*)	3.3×10^{17}	30 000
PbTe (*L*)	1.45×10^{17}	34 500
PbSe (*W*)	5.25×10^{17}	31 000
$Pb_{1-x}Sn_xTe$	9.8×10^{16}	40 000

mainly via polar-optical-phonon scattering which is a highly anisotropic scattering process. Chuenkov[20] and Dumke[21] treated the problem of impact ionization in polar semiconductors. The theory of Dumke which has been very useful in interpreting the generation-rate data of InSb[22] is applied here to the lead chalcogenides. This theory gives a satisfactory picture of the process of impact ionization in narrow-band-gap polar semiconductors such as the $Pb_{1-x}Sn_xTe$ alloys, where the energy gap can be changed appreciably by varying the atomic fraction x.

II. EXPERIMENTAL PROCEDURE

A. Material and Sample Preparation

The lead chalcogenides are cubic semiconductors of the rock-salt crystal structure which are able to exist as stable compounds under fairly wide deviations from stoichiometry. The carrier concentration can be controlled by adjusting the Pb: chalcogen ratio of a pure crystal. This is accomplished by various annealing procedures which have been reviewed recently by Calawa *et al.*[23] The starting ingots are Bridgman grown with high p-type carrier concentrations. Low-concentration PbTe and $Pb_{1-x}Sn_xTe$ are obtained by isothermal annealing,[24] while a two-zone-annealing scheme[25] is used to obtain low concentration PbSe. Table I lists the low-field properties of the various crystals studied, obtained from standard Hall-effect measurements. The rather high carrier concentrations available required special sample geometries shown in Fig. 1. In order to produce sufficient carrier heating, cross sections of typically 40×10^{-6} cm^2 are necessary. For most of the measurements reported here dumbbell-shaped samples (which are obtained by a controlled etching of the center portion of a rectangular bar having at each end an In-alloyed contact) have been used for their mechanical stability, better heat sinking, and electrical properties. The rectangular samples were also used to verify the accuracy of the normalization, but were much more difficult to produce.

The electric field, assumed constant over the etched portion of the sample can be calculated from the total voltage drop across the sample. A suitable geometrical model of the sample is used to calculate the Ohmic voltage drop in the end portions of the sample. An accuracy of ±7% is expected for the determination of the electric field. An error of ±20% is estimated for the absolute value of the drift velocity because of uncertainties in the determination of the carrier concentration n_0 and the cross-sectional area. The excellent agreement obtained between various samples indicates that the use of dumbbell-shaped samples is adequate and solves many problems so often encountered with the use of rectangular parallelepipeds.

B. Experimental Arrangement

The experimental arrangement is shown in Fig. 2. A high-voltage pulser having a characteristic impedance of 50 Ω (SKL Model No. 500) and operated by a mercury-wetted-contact relay in conjunction with a high-voltage power supply (0–4000 V) is used to generate voltage pulses of up to 2000 V with duration varying from 5 to 100 nsec with a repetition rate of typically 5 Hz. These voltage pulses are transmitted through a 50-Ω coaxial transmission line terminated by the sample under test (typically of the order of 1 Ω) in series with a

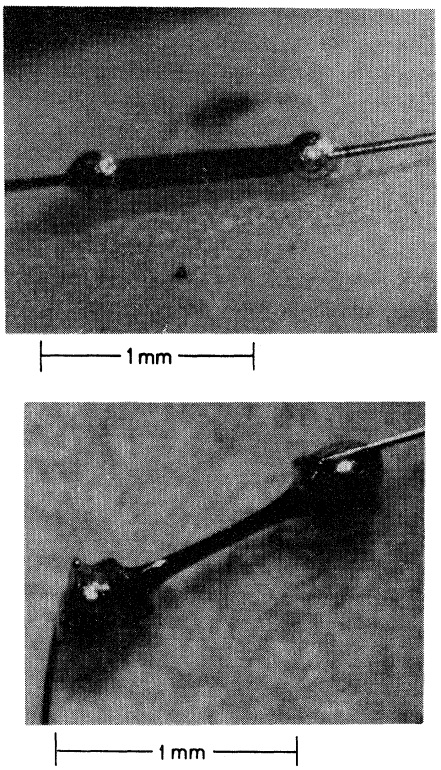

FIG. 1. Samples of PbTe.

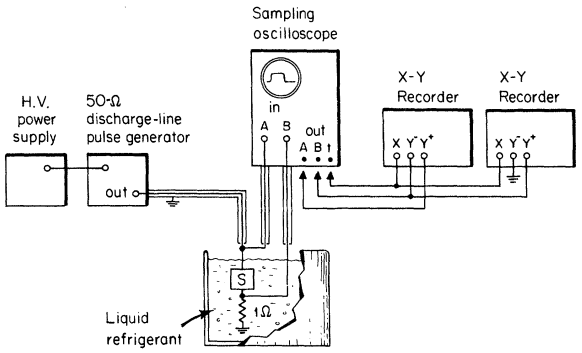

FIG. 2. Experimental arrangement.

1-Ω current-sampling resistor. The sample and resistor are mounted in a low-inductance sample holder. The two measuring voltage probes have a characteristic impedance of 50 Ω and act as high-impedance probes.

III. RESULTS

The results are presented in the form of velocity-field characteristics. They are actually plots of J/n_0e vs E, with n_0 the low-field carrier concentration. When n_0 does not depend on the electric field, J/n_0e is identical to the drift velocity. Unless otherwise stated the velocity-field characteristics presented were measured 5 nsec after the onset of a 10-nsec pulse. Figure 3–5 give the results obtained for PbSe, PbTe, and $Pb_{0.83}Sn_{0.17}Te$, respectively. In all cases a region of saturating velocity is observed, the velocity reaching values close to 1×10^7 cm/sec. This behavior is ascribed to a field-dependent mobility and is similar to results obtained in InSb[3] for fields less than 250 V/cm. The electric fields attained, however, vary considerably from material to material and are a measure of the strength of the polar-optical-phonon interaction.[6] In PbSe (Fig. 3) an inflection point is observed at about 2500 V/cm for both 4.2 and 77 °K. Above that point the current increases more rapidly with increasing electric field, a behavior consistent with the occurrence of carrier multiplication. No explicit time dependence is observed either in the voltage or the current pulse. It was found with the use of pulses longer than 10 nsec that measurable Joule-heating effects occur in the region of electric fields above the inflection point. For this reason it was not possible to identify experimentally the carrier-multiplication process.

Figure 4 shows the results for PbTe. The dashed curve represents the average data obtained from several samples: The full curve is the result of a probe measurement made on a 1-mm-long sample. Three probes (indium-plated platinum wires) were positioned along the etched portion of a sample and then alloyed by passing a current through the small wire. Accurate electric field measurements could then be made; the accuracy of the electric field normalization in this case should be better than 5%. At about 1050 V/cm and 77 °K an instability occurs. If the instantaneous current and voltage are plotted at a particular time during the pulse, it appears as a time-dependent S-type bulk negative differential conductivity (BNDC). The negative slope is actually limited by the 50-Ω load line of the circuit and it was verified with the probe measurement that the electric field remains uniform up to the threshold field, above which nonuniformities could be detected. A more detailed description of the instability has been given elsewhere.[26] At 4.2 °K a stable character-

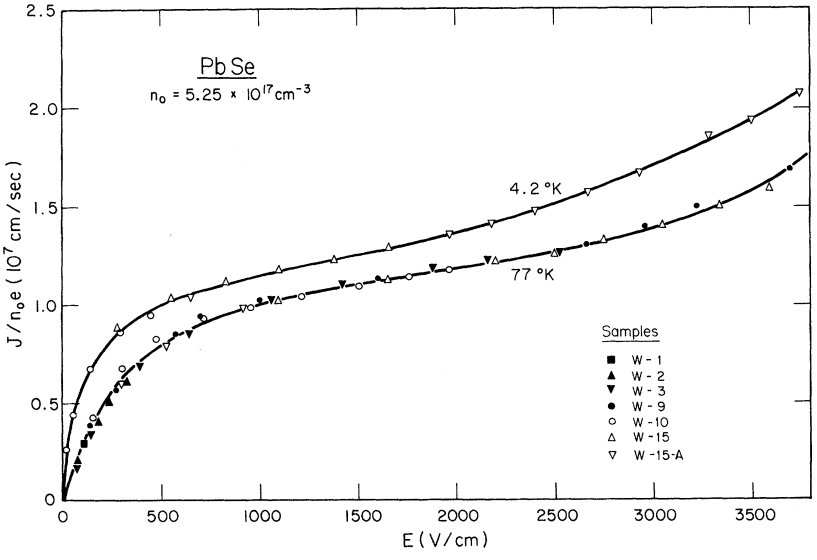

FIG. 3. Velocity-field characteristics of n-type PbSe at 77 and 4.2 °K.

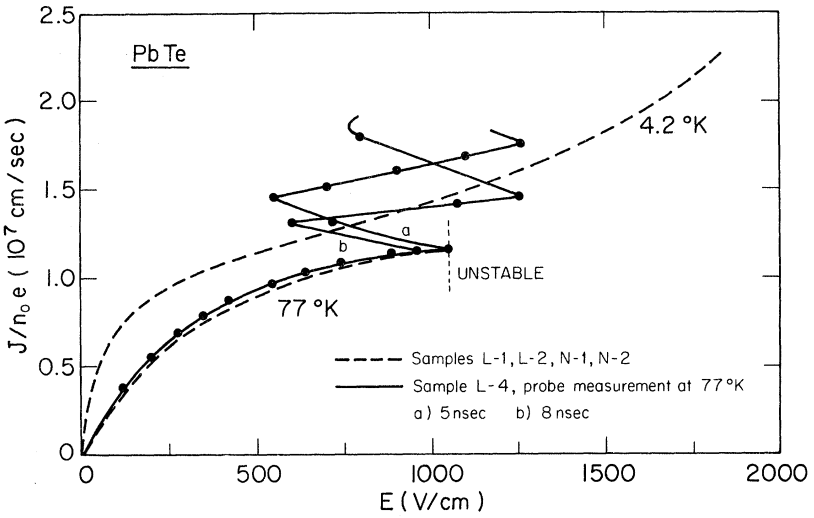

FIG. 4. Velocity-field characteristics of n-type PbTe at 77 and 4.2 °K.

istic is observed with an inflection point around 1000 V/cm.

For $Pb_{0.83}Sn_{0.17}Te$, instabilities are observed at both 4.2 and 77 °K. The threshold fields are however much smaller, being of the order of 550 V/cm at 77 °K. The oscillations observed at 4.2 °K are weaker than those observed at 77 °K as indicated by the envelope curve at 4.2 °K.

The object of the present work is to correlate the experimental inflection points observed in the v-E curves with the onset of impact ionization. It will be shown that in the region of electric fields above the inflection points appreciable impact ionization takes place. The explanation of the velocity-field curve in this region of electric fields is however complicated by the presence of a self-pinching effect. Estimates of the importance of this effect have been reported elsewhere[26] and indicate that it cannot be ignored on the time scale of our experiments. These estimates indicate the possibility of stable as well as unstable voltage-current characteristics in the presence of impact ionization and pinching as have been observed for similar conditions in InSb.[27] Due to a lack of experimental data and due to the complexity of a theoretical model suitable for the Pb chalcogenides the calculations have not been pursued. The present paper is thus chiefly concerned with demonstrating the existence of impact ionization in the lead chalcogenides in the region of electric fields where measurements have been performed. It may serve as a basis for a calculation of the dy-

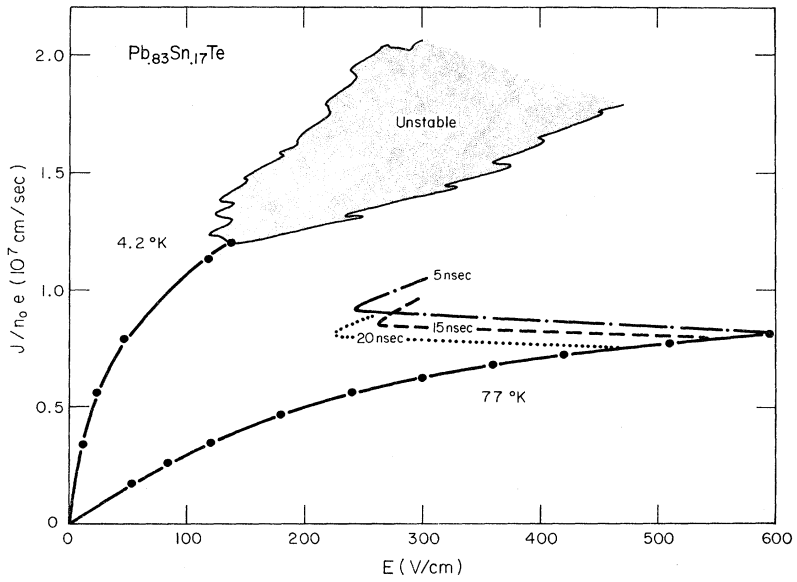

FIG. 5. Velocity-field characteristics of n-type $Pb_{0.83}Sn_{0.17}Te$ at 77 and 4.2 °K.

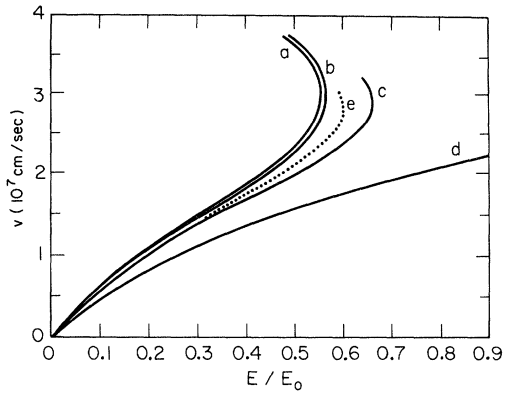

FIG. 6. Theoretical velocity-field characteristic for PbTe at 77 °K obtained from Stratton's model for polar-optical-phonon scattering only (curve a), with nonpolar optical scattering $D = 4.9 \times 10^8$ eV/cm (curve b), 15.5×10^8 eV/cm (curve c), 31×10^8 eV/cm (curve d). The influence of acoustic scattering is shown in curve e. For PbTe the constant E_0 is 3320 V/cm (Ref. 6).

namics of the pinching process.

IV. THEORETICAL

In the following the nature of the velocity-field characteristics below the onset of impact ionization is first reviewed. Then the results of a calculation of the carrier generation rates in the Pb salts are given.

A. Field-Dependent Mobility

The low-field scattering properties of the Pb salts have recently been reviewed by Ravich, Efimova, and Tamarchenko.[28,29] It is well established that polar-optical-phonon scattering is dominant in the range of carrier concentrations between 10^{17} and 5×10^{17} cm^{-3}. A theory of mobility at these concentrations is however complicated due to the necessity of considering screening, nonparabolicity of the energy bands, and because the statistics are neither completely degenerate nor completely classical. In addition, at the temperatures of interest ($T \leq 77$ °K), no single relaxation time exists for this type of scattering which complicates the solution to the Boltzmann equation. Also, if one seeks a precise comparison with experiment, acoustic scattering cannot be completely neglected.

To investigate theoretically deviations from Ohmic behavior in such a system is a formidable task compatible only with modern simulation computing techniques. It was shown in Ref. 6, however, that the features of the v-E characteristics below the inflection points can be explained with the help of a simple theory due to Stratton.[15] This theory assumes that carrier-carrier collisions are sufficiently frequent to randomize both the energy and momentum distributions. The assumed form of the distribution function is that of a Maxwellian displaced in momentum space. Analytically this distribution is especially useful in the treatment of scattering processes for which the relaxation-time approximation does not hold. Stratton was able to obtain simple analytic expressions for the velocity–vs–electric-field relations in the cases of polar-optical-phonon scattering[15] and acoustic- and nonpolar-optical-phonon scattering.[30] Figure 6 shows results calculated for PbTe at 77 °K. The electric field is normalized to the characteristic field E_0 measuring the coupling to polar-optical phonons. Curve (a) is calculated assuming polar-optical-phonon scattering only. Curves (b)–(d) show the influence of nonpolar-optical-phonon scattering for various values of the deformation potential D. As discussed in Ref. 6 these values appear unusually large and thus nonpolar-optical-phonon scattering can be neglected. Curve (e) of Fig. 6 shows the influence of acoustic scattering for $\Xi \simeq 24$ eV for which the contribution of acoustic scattering to the low-field mobility is 10%. The value of 24 eV has been deduced from various transport measurements[31] as a fitting parameter to various experimental results and is much higher than theoretical values obtained from band calculations.[32] The importance of acoustic scattering is probably overestimated and one can conclude from Fig. 6 that polar-optical-phonon scattering is the only important scattering mechanism operating at high electric fields. As shown in Ref. 6 the remarkable feature of Stratton's theory is that it predicts well the scale of the electric fields over which the velocity will tend to saturate. The polar runaway shown in Fig. 6 is only a mathematical result and does not correspond to any physically realizable state.

One can estimate the critical concentrations n_g and n_p required for electron-electron interactions to randomize the energy and momentum distributions, respectively.[33] Because of an uncertainty in the choice of the effective dielectric constant $\bar{\epsilon}$ that screens the e-e interaction, no simple answer can be obtained. One can conclude that while e-e scattering should play a role in our experiments, the drifted Maxwellian is not completely justified and is, thus, not expected to describe accurately the physical processes involved.

B. Impact Ionization

The process of impact ionization in a semiconductor is conveniently described by an electron-hole-pair generation rate g, which measures the number of electron-hole pairs created per particle per unit time in a unit volume of the crystal. One can determine g from the time rate of change of the current in a bulk sample of semiconductor

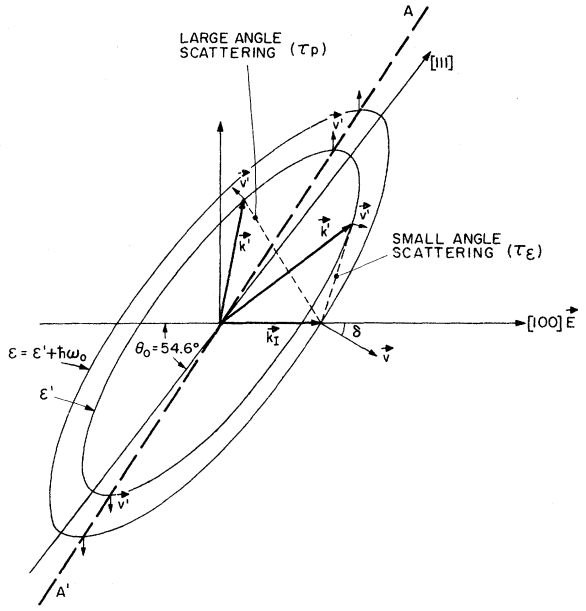

FIG. 7. Constant-energy surfaces of PbTe with the electric field applied in the ⟨100⟩ direction.

subjected to a constant electric field.[22,34] Dumke calculated g for a polar semiconductor having spherical constant-energy surfaces and nonparabolic energy bands and applied the results to InSb and InAs.[21] We modified the calculation to take into account the ellipsoidal constant-energy surfaces of the Pb salts. The major effect of the anisotropy of the band structure is to modify the calculation of the scattering times $\tau_\mathcal{E}$ and τ_p which are, respectively, the energy and momentum relaxation times in the framework of Dumke's theory.

C. Streaming Approximation

The probability of polar scattering from a state with wave vector $\vec{k}$ to a state with wave vector $\vec{k}'$, with the spontaneous emission of a phonon of energy $\hbar\omega_0$ is given by

$$P(\vec{k},\vec{k}') = A[\delta(\mathcal{E}' + \hbar\omega_0 - \mathcal{E})/|\vec{q}|^2] , \qquad (1)$$

where A is a constant measuring the strength of the interaction and $\vec{q}$ is the phonon wave vector. Figure 7 illustrates a constant-energy surface in PbTe with the applied electric field in the ⟨100⟩ direction. The $1/q^2$ dependence in Eq. (1) causes small-angle scattering to be favored over large-angle scattering. As a result in a strong electric field an electron will continue to move in the direction of the field after each collision and will continue to gain energy from the field. Consider an electron in state $\vec{k}_I$ parallel to the electric field. By analogy with the spherical case we define a small-angle-scattering event as an event that puts the electron in a state $\vec{k}'$ where it is accelerated again by the field ($\vec{v}' \cdot \vec{E} > 0$). A large-angle-scattering event, on the other hand, puts the electron in a state where it is decelerated by the field ($\vec{v}' \cdot \vec{E} < 0$). The condition $\vec{v}' \cdot \vec{E} = 0$ is the equation of the plane AA' of Fig. 7. The plane AA' separates the two regions of $\vec{k}$ space where large-angle and small-angle scattering occur, respectively. We define the scattering rates $1/\tau_\mathcal{E}$ and $1/\tau_p$ as the total probabilities of small-angle and large-angle scattering, respectively. $1/\tau_\mathcal{E}$ is obtained by integrating $P(\vec{k}_I, \vec{k}')$ over all states $\vec{k}'$ to the right of AA'. For τ_p the integration is done over all states $\vec{k}'$ to the left of AA'.

Since $\tau_\mathcal{E}$ is much smaller than τ_p it follows that the energy relaxation will be controlled by $\tau_\mathcal{E}$ almost exclusively. On the other hand after a large-angle-scattering event the electron is decelerated continuously to lower energies until it reenters the distribution with a positive velocity with respect to the field. Consequently, the relaxation of the distribution is controlled by τ_p. The validity of the streaming approximation is discussed in Appendix A. The streaming approximation is equivalent to assuming that in k space all electrons have wave vectors in the $\vec{k}_I$ or ⟨100⟩ direction. One can then calculate the probabilities $1/\tau_\mathcal{E}$ and $1/\tau_p$, and the distribution in energy $n(\mathcal{E})$ from which the generation rate is calculated.

D. Generation-Rate Calculation

A simple two-band Kane model is used to treat the nonparabolicity of the conduction and valence band. The energy dispersion relation is given by

$$\mathcal{E}(1 + \mathcal{E}/\mathcal{E}_g) = \hbar^2(k_t^2/m_t + k_l^2/m_l) . \qquad (2)$$

Dubrovskaya *et al.*[35] were able to obtain reliable values for the constants of the model at 77 °K from various thermoelectric measurements. These measurements yielded values of masses and energy gap in very good agreement with the 4.2 °K band-edge parameters determined by Cuff *et al.*,[36] and the 4.2 °K energy gaps of these materials. These values, given in Table II, are used in all calculations performed here.

The integration of $P(\vec{k}, \vec{k}')$ with the limits of integration defined by the plane AA' involves various coordinate transformations and was performed numerically on a digital computer. The mathematical details are given in Appendix B. Figure 8 shows the results obtained for the scattering times $\tau_\mathcal{E}$ and τ_p in the case of InSb, PbTe, and PbSe. The result for InSb is shown for comparison since in this material the energy surfaces are spherical. The results indicate that, as the mass anisotropy ratio K increases in going from InSb ($K = 1$) to PbSe ($K = 1.75$) to PbTe ($K = 10$), the ratio

TABLE II. Values of the constants used in the calculation of the generation rate. For comparison, the values used in the case of InSb are also shown (from Ref. 21).

Symbol	InSb	PbSe	PbTe	$Pb_{1-x}Sn_xTe$ $x=0.07$	$x=0.125$	$x=0.17$
$\hbar\omega_0$ (eV)[a]	0.0238	0.0165	0.0136	0.0137	0.0139	0.0141
ϵ_s[b]	17.9	280	450	540	610	670
ϵ_∞[b]	15.7	25.2	36.9	37.4	37.8	38.2
m_t	0.013	0.040[c]	0.024[c]	0.020	0.017	0.014[d]
K	1	1.75[c]	10[c]	10	10	10[d]
E_g (eV), 4.2 °K[e]	0.225	0.165	0.190	0.145	0.110	0.080
E_g (eV), 77 °K[e]	0.215	0.175	0.210	0.164	0.126	0.098
r	21	30	37	36	36	35

[a]R. N. Hall and J. H. Racette, J. Appl. Phys. Suppl. 32, 2078 (1961).
[b]E. Burstein, S. Perkowitz, and M. H. Brodsky, J. Phys. (Paris) Suppl. 29, C4-78 (1968).
[c]Reference 36.
[d]J. Melngailis, T. C. Harman, J. G. Mavroides, and J. O. Dimmock, Phys. Rev. B 3, 370 (1971).
[e]A. J. Strauss, Trans. Met. Soc. AIME 242, 355 (1968).

$\tau_p/\tau_\mathcal{E}$ at high energies changes from 10 to 9 to 6, respectively. These purely geometrical effects are important and could not be taken into account by the use of a spherical effective mass.

The remainder of the calculation proceeds as in the original work of Dumke. The reader is referred to his paper for the details of the treatment. The generation rate g is obtained from the following set of equations:

$$g=\frac{\tau_p(\mathcal{E}_i)[\lambda(\mathcal{E}_i)D_\mathcal{E}(\mathcal{E}_i)-a]\exp[-\int_{\hbar\omega_0}^{\mathcal{E}_i}\lambda(\mathcal{E})\,d\mathcal{E}]}{[\tau_i+\tau_p(\mathcal{E}_i)]\{\hbar\omega_0+\int_{\hbar\omega_0}^{\infty}\exp[-\int_{\hbar\omega_0}^{\mathcal{E}}\lambda(\mathcal{E}')d\mathcal{E}']d\mathcal{E}\}}\,, \tag{3}$$

$$\lambda(\mathcal{E})=a/2D_\mathcal{E}+[(a/2D_\mathcal{E})^2+1/D_\mathcal{E}\tau_p]^{1/2}\,, \tag{4}$$

$$a=\hbar\omega_0/\tau_\mathcal{E}-e\vec{\mathrm{E}}\cdot\vec{\mathrm{v}}\,, \tag{5}$$

$$D_\mathcal{E}=(\hbar\omega_0)^2/2\tau_\mathcal{E}\,. \tag{6}$$

Here τ_i and $\mathcal{E}_i$ are the time for ionization and the minimum energy for ionization, respectively. In these equations the changes brought up by the ellipsoidal energy surfaces appear only in the calculation of $\tau_\mathcal{E}$ and τ_p and in the expression for the velocity $\vec{\mathrm{v}}$ as a function of energy.

The value of $\mathcal{E}_i$ was assumed to be $\frac{3}{2}\mathcal{E}_g$ for the Pb salts. In those materials electron and holes have equal masses so that a simple calculation of $\mathcal{E}_i$ using energy and momentum conservation yields precisely $\frac{3}{2}\mathcal{E}_g$. In InSb, on the other hand, where $m_e \ll m_h$, the value $1.1\mathcal{E}_g$ is more appropriate.[37] The ionization time τ_i was taken to be

$$\tau_i=r(1/\tau_\mathcal{E}+1/\tau_p)^{-1}\,, \tag{7}$$

where r is an estimate of the average number of phonons emitted for each impact-ionization event. Klein[38] recently reviewed the theory of radiation-ionization energies in semiconductors. He found that the phonon energy loss $r\hbar\omega_0$ required for the creation of an electron-hole pair does not vary appreciably with the energy gap of the semiconductor and is of the order of 0.5 eV for most semiconductors. To the knowledge of the authors there are no published values of the energy loss term for the Pb salts. Hence, a value of 0.5 eV is assumed here.

Table II lists values of the various constants used in the theory. For the PbSn salts a linear interpolation between $x=0.17$ and $x=0$ was used for the values of m_t at $x=0.125$ and $x=0.07$. The anisotropy ratio K is assumed to be 10 in all mixed crystals considered. The constants ω_0, ϵ_s, and ϵ_∞ were linearly interpolated between PbTe and SnTe for the mixed crystals.

The theoretical treatment described so far is

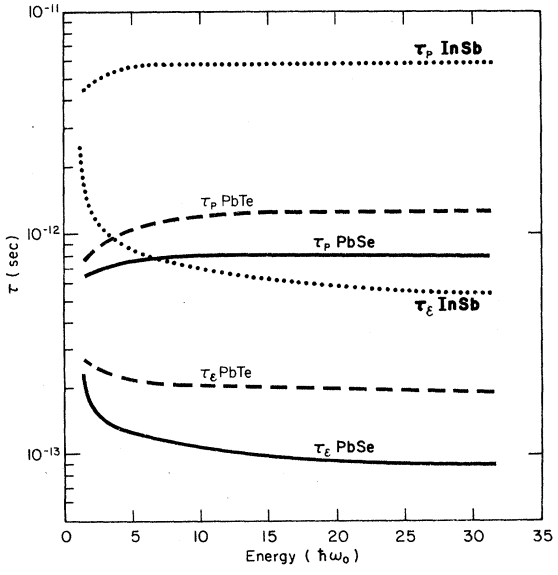

FIG. 8. Large-angle (τ_p) and small-angle ($\tau_\mathcal{E}$) scattering time for PbSe, PbTe, and InSb.

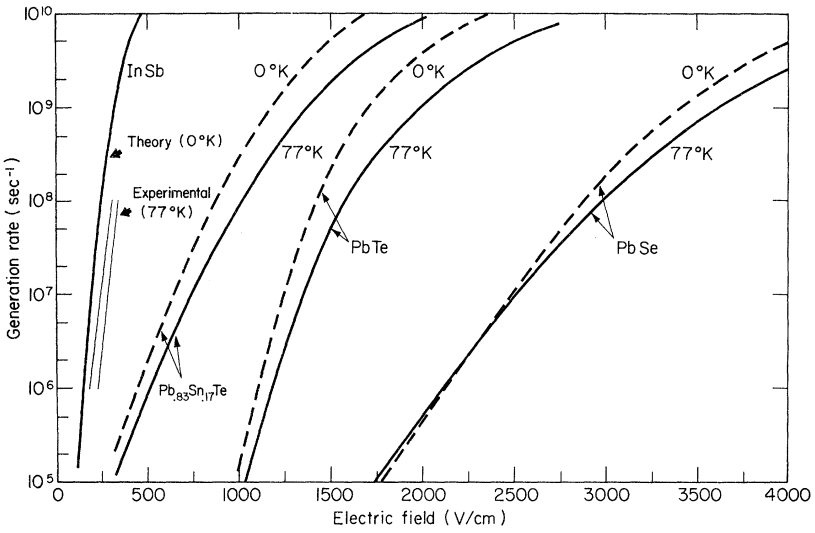

FIG. 9. Theoretical generation rates in PbSe, PbTe, and $Pb_{0.83}Sn_{0.17}Te$. The results for InSb are from Ref. 21.

valid only for $T = 0$ °K, i.e., the scattering occurs only through spontaneous emission of phonons. At higher temperatures the optical modes are partially excited and phonon absorption as well as stimulated emission of phonons can occur. Dumke has shown that these effects are taken into account if τ_p and $D_\mathcal{E}$ are replaced by $\tau_p(0)/(1+2n_q)$ and $D_\mathcal{E}(0)(1+2n_q)$, respectively. Here n_q is the boson occupation number at a temperature T. The calculations were performed by numerical integration. The energy grid size was taken to be $0.1\hbar\omega_0$ and a range of energies from 0 to $60\hbar\omega_0$ ensured excellent convergence.

E. Results and Discussion

The results of the calculation of g are shown in Fig. 9. The result for InSb was obtained by Dumke.[21] For the lead salts, the 0 and 77 °K calculations yield basically similar results. This reflects the fact that the band-structure parameters of the modified Kane model are assumed to be the same in both cases, i.e., the 4.2 °K masses and band gaps are used at 77 °K as well. The differences between the 0 and 77 °K calculations originate mainly from $\mathcal{E}_i$ and the factor $(1+2n_q)$ defined above.

If we compare the generation rates calculated for PbSe and PbTe we find that impact ionization will occur at lower fields in PbTe even though $\mathcal{E}_i$ is slightly larger, reflecting the weaker coupling to polar-optical phonons in this material. The strength of the polar-optical-phonon interaction is measured by the constant A of Eq. (1). The value of A, given in Appendix B, is proportional to $(\epsilon_\infty^{-1} - \epsilon_s^{-1})$. As seen from Table II, this value is approximately the same for PbTe and the PbSn salts while differing appreciably in PbSe and InSb. The generation rate for $Pb_{0.83}Sn_{0.17}Te$ at a given electric field is much higher than for PbTe, indicating that the reduction in band gap for the same coupling to the phonon system increases considerably the probability of impact ionization.

TABLE III. Comparison between theory and experiment.

Semicond.	(°K)	Expt. inflection point (V/cm)	Theory $g = 10^6 \rightarrow 10^7$ sec^{-1}
PbSe	77	2500 (stable)	2150 → 2500
	4.2	2200 (stable)	2150 → 2500
PbTe	77	1050 (unstable)	1200 → 1350
	4.2	1000 (stable)	1100 → 1250
$Pb_{0.83}Sn_{0.17}Te$	77	550 (unstable)	500 → 750
	4.2	140 (unstable)	450 → 650

In order to compare the generation-rate calculation with the experimental results we define arbitrarily the onset of impact ionization as $g = 10^6$ sec^{-1}. For the time scale of our experiment (5 nsec), this value of g is equivalent to changes of a few percent in the macroscopic circuit variables, current, and voltage, and thus is useful in defining the onset of observable impact ionization. Table III gives the values of the electric fields at the various experimental inflection points and for comparison the fields at $g = 10^6$ and $g = 10^7$ sec^{-1}. The correlation between theory and experiment is very good, whether the experimental inflection points are followed by a stable or an unstable J-E characteristic. The only important disagreement occurs for $Pb_{0.83}Sn_{0.17}Te$ at 4.2 °K. This could result from the temperature dependence of the constants of the band model and will not be investigated further.

Figure 10 shows the results of a calculation for $Pb_{1-x}Sn_xTe$ with $x = 0.07$ and $x = 0.125$. Curves of constant g are plotted as a function of electric field and atomic fraction x. For comparison we

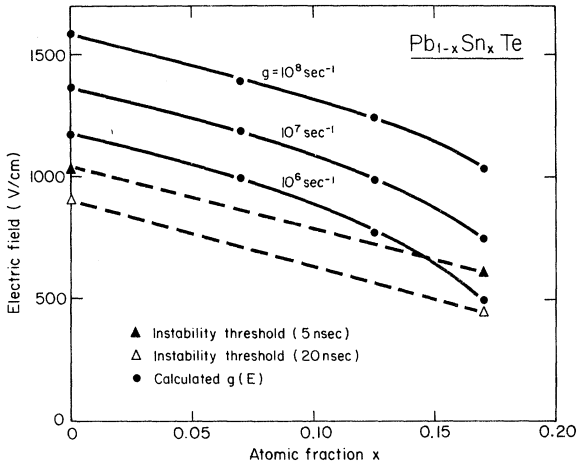

FIG. 10. Generation-rate calculations for $Pb_{1-x}Sn_xTe$ at 77 °K. For comparison the threshold electric fields of the instability in PbTe and $Pb_{0.83}Sn_{0.17}Te$ are shown.

have shown the thresholds of the instability observed in PbTe and $Pb_{0.83}Sn_{0.17}Te$. If the experimental points are joined by straight lines we see that the slope of these lines are approximately equal to the slopes of the constant generation rate curves, which could indicate that the threshold of the instability at a given time after the onset of the pulse occurs at a fixed generation rate. This is consistent with the instability threshold corresponding to the onset of impact ionization. From the shapes of the constant-g curves near $x = 0.17$, one could expect very low thresholds at $x > 0.17$, as a result of the zero-band-gap crossing near $x \simeq 0.35$.

The drift velocity can be evaluated from the integral $\int |\vec{v}| \cos(\delta) n(\mathcal{E}) d\mathcal{E}$, where $n(\mathcal{E})$ is the calculated distribution function and $|\vec{v}|$ and $\cos\delta$ are given by Eqs. (8) and (9). The results for PbTe and PbSe indicate that the experimental velocities are roughly 50% of the calculated values, indicating that the electron distribution is not completely streamed. A less anisotropic distribution in the Pb salts could result from the influence of electron-electron interactions. As seen above, carrier-carrier collisions cannot be neglected in material of 10^{17} cm^{-3}.

In fact, the drift velocities predicted by Stratton's model which assumes a nearly isotropic distribution are in better agreement with the experiment than those predicted by Dumke's theory. These qualitative arguments, however, do not minimize the importance of the generation-rate calculations, in view of the many approximations that need to be made in these theories. Since g is such a sharply rising function of electric field, it should not be very sensitive to the exact shape of the distribution.

V. CONCLUSION

The experimental and theoretical results presented here confirm the existence of impact ionization at fields above 550, 1050, and 2500 V/cm in $Pb_{0.83}Sn_{0.17}Te$, PbTe, and PbSe, respectively. It was shown that both the strength of the polar-optical-phonon interaction and the relative size of the energy gap determine the effective threshold for impact ionization. The theory of Dumke, assuming a distribution function streamed in the direction of the field, seems appropriate to describe impact ionization in narrow-band-gap polar semiconductors.

ACKNOWLEDGMENTS

It is a pleasure to thank R. H. Rediker for many helpful discussions. The authors also wish to thank A. J. Strauss and T. C. Harman for supplying some crystals of PbTe and $Pb_{0.83}Sn_{0.17}Te$. The computations were carried out at the MIT Information Processing Center.

APPENDIX A: DIRECTION OF STREAMING

We consider here the direction of $\vec{k}$ space in which the distribution function is assumed to stream. In order to cause impact ionization, electrons must gain more energy than they lose by small-angle scattering. A measure of the average energy gained from the field between collisions is given by $(\vec{E} \cdot \vec{v})\tau_{\mathcal{E}}$. In Fig. 11, the rate of energy

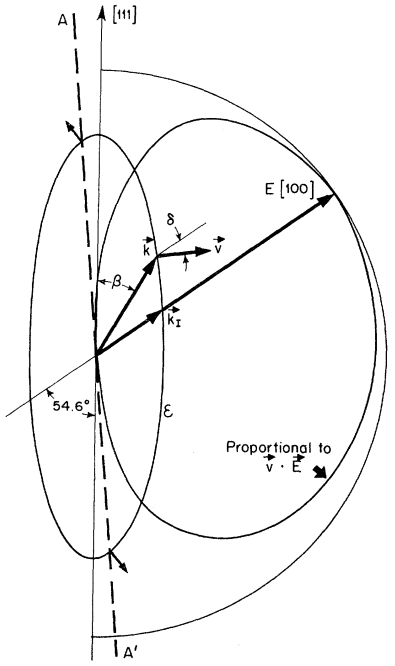

FIG. 11. Rate of energy gain from electric field as a function of position along the surface of constant energy.

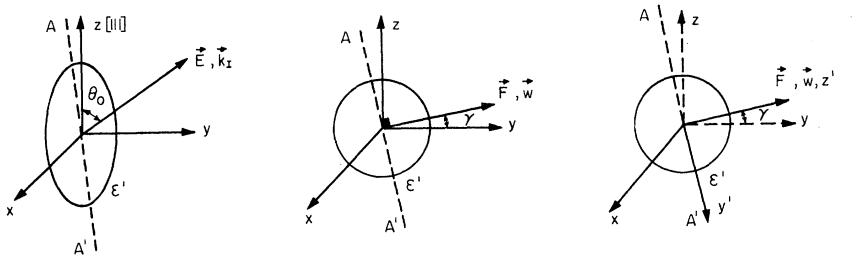

(a) $(\vec{k},\vec{v})$ space (b) $(\vec{w},\vec{u})$ space (c) $(\vec{w},\vec{u})$ space rotated around x axis

FIG. 12. Various coordinate transformations used in the theory.

gain $\vec{E}\cdot\vec{v}$ is plotted in polar coordinates as a function of angular position β along the ellipsoid. It can be shown that the component of $\vec{v}$ along the electric field is given by $|\vec{v}|\cos\delta$ with

$$|\vec{v}| = \left(\frac{2\mathcal{E}_G}{m_t}\right)^{1/2} \frac{[(\mathcal{E}/\mathcal{E}_G)(1+\mathcal{E}/\mathcal{E}_G)]^{1/2}}{(1+2\mathcal{E}/\mathcal{E}_G)} \times \left(1-\frac{(K-1)\cot^2\beta}{K(K+\cot^2\beta)}\right)^{1/2}, \quad (8)$$

$$\delta = \tan^{-1}(K\tan\beta) - \theta_0 , \quad (9)$$

where the angles β and δ are defined in Fig. 11, which shows that $\vec{v}\cdot\vec{E}$ is maximum for the wave vector $\vec{k}_I$. If we assumed $\tau_\mathcal{E}$ to be independent of the angular position, then the result of Fig. 11 would indicate that the energy gain from the field in an average collision would be largest for electrons with wave vectors parallel to the field and that these electrons would contribute the most to the ionization process. For ellipsoidal energy surfaces the scattering rates $1/\tau_\mathcal{E}$ and $1/\tau_p$ are a function of the angular position β. Since long computing time would be required to find the β direction of maximum $\tau_\mathcal{E}$, we made a single calculation of $\tau_\mathcal{E}$ at an angle β other than 54.6°. The angle chosen was 8°, at which the velocity vector v is parallel to the field. It was found that $\tau_\mathcal{E}$ was largest along the $\vec{k}_I$ direction. In fact, the quantity $(\vec{v}\cdot\vec{E})\tau_\mathcal{E}$ is about three times larger for electrons in state $\vec{k}_I$ than for electrons in the initial direction $\beta = 8°$. This result reflects the fact that electrons in the direction $\vec{k}_I$ have an effective mass very close to the transverse mass m_t and are, therefore, more easily accelerated in the electric field. Since the effective mass is very close to m_t and varies very slowly with β for directions in the neighborhood of $\vec{k}_I$, we simply assume the distribution to stream along $\vec{k}_I$.

APPENDIX B: CALCULATION OF $\tau_\mathcal{E}$ AND τ_p

In this section we calculate $\tau_\mathcal{E}$ and τ_p for the case where the initial wave vector $\vec{k}$ is in the direction of the applied electric field.

We shall make transformations from the $(\vec{k}, \vec{v})$ space to the $(\vec{w}, \vec{u})$ space in which the energy surfaces are spherical. In these transformations the wave vector $\vec{k}$ becomes $\vec{w}$, and the velocity $\vec{v}$ becomes $\vec{u}$. The transformation is illustrated in Figs. 12(a) and 12(b) and is given by

$$\vec{k} = \overleftrightarrow{T}\vec{w}, \quad \vec{v} = \overleftrightarrow{T}^{-1}\vec{u},$$

$$\overleftrightarrow{T} = \begin{pmatrix} 1 & 0 & 0 \\ 0 & 1 & 0 \\ 0 & 0 & \sqrt{K} \end{pmatrix}, \quad (10)$$

where K is the anisotropy ratio. Upon transformation the energy dispersion becomes

$$(\hbar^2/2m_t)(k_t^2 + k_z^2/K) = \hbar^2 w^2/2m_t , \quad (11)$$

while the dot product $\vec{v}'\cdot\vec{E}$ becomes $\vec{u}'\cdot\vec{F}$, where $\vec{F}$ is the electric field obtained by the transformation

$$\vec{E} = \overleftrightarrow{T}\vec{F} . \quad (12)$$

Referring to Fig. 7, the small-angle scattering rate $1/\tau_\mathcal{E}$ is simply given by $P(\mathcal{E})$ with

$$P(\mathcal{E})\,d\mathcal{E} = \int \int_{\substack{\text{Surface to} \\ \text{the right} \\ \text{of } AA'}} P(k,k')\,dV_{k'}\,(2\pi)^{-3} . \quad (13)$$

In the $(\vec{w}, \vec{u})$ space, the plane AA' is given by $\vec{u}'\cdot\vec{F} = 0$ or, equivalently, $\vec{w}'\cdot\vec{F} = 0$, since now $\vec{w}'$ and $\vec{u}'$ are parallel. This plane [see Fig. 12(b)] separates the sphere of constant energy into two hemispheres over which the integration will be performed. Using Eq. (1) we can write Eq. (13) as

$$P(\mathcal{E})\,d\mathcal{E} = \frac{A\sqrt{K}}{(2\pi)^3} \iint_{\substack{\text{Surface to the} \\ \text{right of } AA'}} \frac{dV_{w'}}{q^2} . \quad (14)$$

If the rotation illustrated in Fig. 12(c) is made, then $\vec{w}$ becomes the z axis of a new spherical system with θ the angle between $\vec{w}$ and $\vec{w}'$. Then $1/\tau_\mathcal{E}$ is given by

$$\frac{1}{\tau_\mathcal{E}} = \frac{A\sqrt{K}}{(2\pi)^3} \frac{w'^2}{|\nabla_{w'}\mathcal{E}|} \int_0^{2\pi} d\phi \int_0^{\pi/2} \frac{\sin\theta\,d\theta}{q^2} . \quad (15)$$

The last step is to express q^2 in the coordinate system of Fig. 12(c). In the $(\vec{k}, \vec{v})$ space, we have

$$q^2 = k^2 + k'^2 - 2\vec{k}\cdot\vec{k}' \,. \tag{16}$$

In the $(\vec{w}, \vec{u})$ space (see Ref. 39), we have

$$q^2 = w^2 + w'^2 - 2ww'\cos\theta + (K-1)(w_z - w_z')^2 \,. \tag{17}$$

In the rotated $(\vec{w}, \vec{u})$ space, we have

$$\begin{aligned} w_z &= w\sin\gamma \,, \\ w_z' &= w'(\cos\theta\sin\gamma - \sin\theta\sin\phi\cos\gamma) \,, \end{aligned} \tag{18}$$

where the angle γ is determined with the help of Eqs. (12) and given by

$$\tan\gamma = F_z/F_y = E_z/\sqrt{K}E_y = \cot\theta_0/\sqrt{K} \,. \tag{19}$$

Rewriting Eq. (15) in terms of $\alpha = w'/w$ and using Eqs. (17) and (18) we find, noting that $\nabla_{w'}\mathcal{E} = \hbar u'$,

$$\begin{aligned} 1/\tau_{\mathcal{E}} &= [A\sqrt{K}\,\alpha^2/(2\pi)^3\hbar u']I_0 , \\ I_0 &= \int_0^{2\pi} d\phi \int_0^{\pi/2} d\theta\,[\sin(\theta)/F(\theta,\phi)] \,, \\ F(\theta,\phi) &= 1 + \alpha^2 - 2\alpha\cos\theta + (K-1)\sin^2\gamma[1 - \alpha\cos\theta \\ &\quad + \alpha\sin(\theta)\sin(\phi)\cot(\gamma)]^2 \,, \\ u' &= \left(\frac{2\mathcal{E}_G}{m_t}\right)^{1/2} \frac{[(\mathcal{E}'/\mathcal{E}_G)(1+\mathcal{E}'/\mathcal{E}_G)]^{1/2}}{1+2\mathcal{E}'/\mathcal{E}_G} \,, \\ A &= 4\pi^2 e^2\omega_0(\epsilon_\infty^{-1} - \epsilon_s^{-1}) \,. \end{aligned} \tag{20}$$

In order to calcuate τ_p the θ integral is performed between $\frac{1}{2}\pi$ and π. The integral I_0 cannot be performed analytically and was therefore computed numerically on a digital computer. The parameter α depends on energy, so that Eqs. (20) yield $\tau_{\mathcal{E}}$ and τ_p as a function of energy.

---

†Work supported by the Office of Naval Research.

*Present address: Hydro-Quebec Institute of Research, Varennes, Quebec, Canada.

‡Present address: Lincoln Laboratory, Lexington, Mass. 02173.

[1]D. M. Chang and J. G. Ruch, Appl. Phys. Letters 12, 111 (1968).

[2]V. Rodgriguez and M. A. Nicolet, J. Appl. Phys. 40, 496 (1969).

[3]M. Glicksman and W. A. Hicinbothem, Jr., Phys. Rev. 129, 1572 (1963).

[4]A. G. Foyt and A. L. McWhorter, IEEE Trans. Electron. Devices ED-13, 79 (1966).

[5]J. B. Gunn, Solid State Commun. 1, 88 (1963).

[6]H. St-Onge, J. N. Walpole, and R. H. Rediker, *Proceedings of the Tenth International Conference on the Physics of Semiconductors, Cambridge, Massachusetts*, 1970, edited by S. P. Keller, J. C. Hensel, and F. Stern (U. S. AEC, Oak Ridge, Tenn., 1970).

[7]Preliminary results have been reported by H. St-Onge and J. N. Walpole, Bull. Am. Phys. Soc. 16, 1416 (1971).

[8]E. M. Conwell, in *Solid State Physics*, edited by F. Seitz, D. Turnbull, and H. Ehrenreich (Academic, New York, 1967), Suppl. 9.

[9]J. E. Smith, M. I. Nathan, J. C. McGroddy, S. A. Porowski, and W. Paul, Appl. Phys. Letters 15, 242 (1969).

[10]T. Kurosawa, J. Phys. Soc. Japan Suppl. 21, 424 (1966).

[11]H. D. Rees, J. Phys. Chem. Solids 30, 643 (1969).

[12]W. Fawcett, A. D. Boardman, and S. Swain, J. Phys. Chem. Solids 31, 1963 (1970).

[13]W. Fawcett and J. G. Ruch, Appl. Phys. Letters 15, 368 (1969).

[14]E. G. S. Paige, IBM J. Res. Develop. 5, 562 (1969).

[15]R. Stratton, Proc. Phys. Soc. (London) A246, 406 (1958).

[16]W. Shockley, Solid State Electron. 2, 35 (1961).

[17]P. A. Wolff, Phys. Rev. 95, 1415 (1954).

[18]G. A. Baraff, Phys. Rev. 133, A26 (1964).

[19]L. V. Keldysh, Zh. Eksperim. i Teor. Fiz. 48, 1692 (1965) [Sov. Phys. JETP 21, 1135 (1965)].

[20]V. A. Chuenkov, Fiz. Tverd. Tela 9, 48 (1967) [Sov. Phys. Solid State 9, 35 (1967)].

[21]W. P. Dumke, Phys. Rev. 167, 783 (1968).

[22]J. C. McGroddy and M. I. Nathan, J. Phys. Soc. Japan Suppl. 21, 437 (1966).

[23]A. R. Calawa, T. C. Harman, M. Finn, and P. Youtz, Trans. Met. Soc. AIME 242, 374 (1968).

[24]R. F. Brebrick and R. S. Allgaier, J. Chem. Phys. 32, 1826 (1960).

[25]N. Ohashi and K. Igaki, Trans. Japan Inst. Met. 5, 94 (1964).

[26]H. St-Onge, F. J. Leonberger, and J. N. Walpole, in Proceedings of the Conference on the Physics of IV-VI Compounds and Alloys, 1972 (unpublished); J. Nonmetals (to be published).

[27]M. Glicksman and M. C. Steele, Phys. Rev. Letters 2, 461 (1959).

[28]Uu. I. Ravich, B. A. Efimova, and V. I. Tamarchenko, Phys. Status Solidi 43(b), 11 (1971).

[29]Yu. I. Ravich, B. A. Efimova, and V. I. Tamarchenko, Phys. Status Solidi 43(b), 453 (1971).

[30]R. Stratton, in *Solid State Physics in Electronics and Telecommunications*, edited by M. Desirant and J. L. Michiels (Academic, New York, 1960), Vol. 1, p. 343.

[31]Yu. I. Ravich, B. A. Efimova, and I. A. Smirnov, *Semiconducting Lead Chalcogenides*, edited by L. S. Stil'bans (Plenum, New York, 1970).

[32]L. G. Ferreira, Phys. Rev. 137, A1601 (1965).

[33]Using values determined by Stratton, one finds for PbTe $n_{\mathcal{E}} \simeq 1.37\times10^{14}\bar{\epsilon}^2$; for $\bar{\epsilon} = \epsilon_\infty = 37$, $n_{\mathcal{E}} = 1.9\times10^{17}$ cm^{-3}; and for $\bar{\epsilon} = \epsilon_s = 400$, $n_{\mathcal{E}} = 2.2\times10^{19}$ cm^{-3}. The calculation of n_p is similar and yields values smaller than $n_{\mathcal{E}}$. We can estimate $\bar{\epsilon}$ from the following. An electron interacting with the lattice experiences the various screened Coulomb potentials of the ions and will travel with a velocity v_T a distance equal to a screening radius r_s in r_s/v_T sec or $1/\omega_p$ sec, where ω_p is the plasma frequency. In PbTe of 10^{17} cm^{-3}, $1/\omega_p = 7.6\times10^{-14}$ sec and a period of lattice vibrations, $2\pi/\omega_0$, is equal to 3×10^{-13} sec. Thus an electron will "see" the lattice very quickly and will polarize mostly core electrons; consequently, an appropriate value of $\bar{\epsilon}$ should lie closer to ϵ_∞ than to ϵ_s, i.e., $\epsilon_\infty < \bar{\epsilon} < \epsilon_s$.

[34]V. L. Dalal, Appl. Phys. Letters 15, 379 (1969).

[35]I. N. Dubrovskaya, Yu. I. Ravich, and O. S. Gryaznov, Fiz. Tekhn. Poluprov. 3, 1770 (1969) [Sov. Phys. Semicond. 3, 1500 (1970)].
[36]K. F. Cuff, M. R. Ellett, C. D. Kuglin, and L. R. Williams, in *Proceedings of the Seventh International Conference on Physics of Semiconductors, Paris*, 1964, edited by M. Hulin (Dunod, Paris, 1964), Vol. I, p. 678.
[37]J. C. McGroddy, in Ref. 6.
[38]C. A. Klein, Phys. Rev. 39, 2029 (1968).
[39]D. J. Olechna and H. Ehrenreich, J. Phys. Chem. Solids 23, 1513 (1962).

PHYSICAL REVIEW B VOLUME 6, NUMBER 6 15 SEPTEMBER 1972

Determination of the Deformation-Potential Constant of the Conduction Band of Silicon from the Piezospectroscopy of Donors*

V. J. Tekippe,† H. R. Chandrasekhar, P. Fisher, and A. K. Ramdas
Department of Physics, Purdue University, Lafayette, Indiana 47907
(Received 1 March 1972)

A piezospectroscopic study of the Lyman spectra of arsenic, antimony, phosphorus, and magnesium donors in silicon has been made using a quantitative-stress cryostat. Within experimental error, all four impurities yield the same value for the shear-deformation-potential constant Ξ_u of the $\langle 100 \rangle$ conduction-band minima. The average value of Ξ_u thus obtained is 8.77 ± 0.07 eV. The shift of the $1s(A_1)$ ground state under stress is characterized by a value of Ξ_u which is lower than the above, viz., 8.3, 8.1, and 7.0 eV for antimony, phosphorus, and arsenic, respectively.

I. INTRODUCTION

Piezospectroscopic studies of the excitation spectra associated with donors and acceptors in semiconductors have proved to be very useful in establishing the site symmetries of the impurities and in providing a symmetry classification of the impurity states.[1] If, in addition, a quantitative stress is employed in such experiments, the deformation-potential constants may be determined for both the ground and excited states. To the extent that these states are described in terms of the band structure,[2] i.e., the conduction-band minima for the donor states and the valence-band maximum for acceptor states in silicon and germanium, these deformation-potential constants should be closely related to the corresponding deformation-potential constants of the band extrema.[3,4] For the donor states, in the effective-mass approximation,[3] these constants should be exactly equal to those of the conduction-band minima, whereas for acceptors they have been shown to be related through numerical factors to those of the valence-band maximum.[4] For silicon, Krag *et al.*[5,6] have reported values for the shear-deformation-potential constant of the conduction-band minima Ξ_u from the piezospectroscopic studies of sulphur, phosphorus, and bismuth donors. These values range from 7.1 to 7.9 eV and differ significantly from the 11-eV value determined by Wilson and Feher[7] and Watkins and Ham[8] using electron-paramagnetic-resonance (EPR) measurements on group-V and lithium donors, respectively. Also, the value for Ξ_u determined by a variety of other techniques lies in the range 8–9 eV (see Table I). We have designed and constructed a quantitative-stress cryostat and have measured Ξ_u from the piezospectroscopic effects of the Lyman spectra of donors in silicon. The present paper reports the results of this investigation.

II. EXPERIMENTAL APPARATUS AND PROCEDURE

The Perkin-Elmer double-pass monochromator (Model No. 112 G) and its associated entrance and exit optics used in these measurements have been described elsewhere.[9] The quantitative-stress cryostat utilized is an adaptation of a glass cryostat used for a number of years in our laboratory (see Fig. 1).[10] The modification consists of replacing the glass centerpiece by one of stainless steel designed to allow an adjustable uniaxial compression to be applied to the sample. The stress centerpiece was also designed to give quantitative information about the stress, very low frictional losses, good cryogenic contact between the sample and the coolant, and a reasonable length of coolant time. In addition, the design parameters allowed for a force in excess of 1×10^8 dyn to be applied to the sample under study.

Figure 2 shows the stress centerpiece; details of the upper and lower sections are shown in Figs. 3 and 4, respectively. The centerpiece is mated to the optical cryostat by means of the stainless-steel cone joint[11] *G*. The pressure head[12] *B* is pressurized with nitrogen gas through the port *A* and the resultant force produced by the piston is transmitted by a hollow push rod *H* which passes through the coolant *I* and makes contact with the

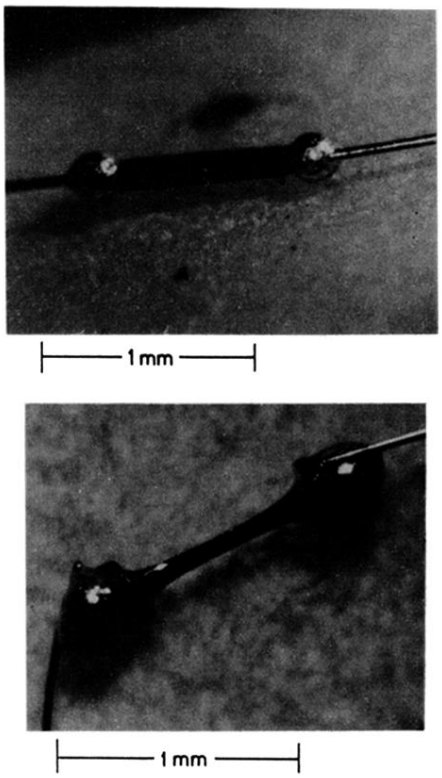

FIG. 1. Samples of PbTe.